Geometric isomerization of dietary monounsaturated fatty acids by a cis/trans fatty acid isomerase from Pseudomonas putida KT2440

Geometric isomerization of dietary monounsaturated fatty acids by a *cis*/*trans* fatty acid isomerase from *Pseudomonas putida* KT2440

Jun-Young Park[a,1], Min-Gyeong Lee[b,1], Dimitris Charalampopoulos[c], Kyung-Min Park[b,*], Pahn-Shick Chang[a,d,e,f,*]

[a] *Department of Agricultural Biotechnology, Seoul National University, Seoul 08826, Republic of Korea*

[b] *Department of Food Science and Biotechnology, Wonkwang University, Iksan 54538, Republic of Korea*

[c] *Department of Food and Nutritional Sciences, University of Reading, Reading RG6 6AP, United Kingdom*

[d] *Research Institute of Agriculture and Life Sciences, Seoul National University, Seoul 08826, Republic of Korea*

[e] *Center for Food and Bioconvergence, Seoul National University, Seoul 08826, Republic of Korea*

[f] *Center for Agricultural Microorganism and Enzyme, Seoul National University, Seoul 08826, Republic of Korea*

[1] Equal contribution as first authors.

* Authors to whom correspondence should be addressed: K. M. Park [telephone: +82 63 850 6681; e-mail: kmpark79@wku.ac.kr] or P. S. Chang [telephone: +82 2 880 4852; e-mail: pschang@snu.ac.kr].

Abstract

Pseudomonas putida KT2440 encodes a defense system that rigidifies membranes by a cytochrome *c*-type *cis*/*trans* fatty acid isomerase (CTI). Despite its potential as an industrial biocatalyst for directly regulating the geometric isomerism of monounsaturated fatty acids, its original catalytic and structural properties have remained elusive. In this study, the catalytic nature of wild-type CTI purified *P. putida* KT2440 against dietary monounsaturated fatty acids was investigated. It showed substrate preference for palmitoleic acid ($C_{16:1}$, *cis*-Δ^9), along with substrate promiscuity with chain length and double bond position (palmitoleic acid>*cis*-vaccenic acid>oleic acid). Under determined optimum reaction conditions, its catalytic efficiency (k_{cat}/K_m) was evaluated as 5.13×10^2 $M^{-1}\cdot sec^{-1}$ against palmitoleic acid. Furthermore, computational predictions of the protein structure revealed its monoheme cytochrome *c*-type domain and a parasol-like transmembrane domain, suggesting its catalytic mode of action. For effective *cis*/*trans* isomerization, the ethylene double bond of monounsaturated fatty acids should be precisely positioned at the heme center of CTI, indicating that its substrate specificity can be determined by the alkyl chain length and the double bond position of the fatty acid substrates. These findings shed light on the potential of CTI as a promising biocatalyst for the food and lipid industry.

Keywords: *cis*/*trans* fatty acid isomerase; cytochrome *c*-type hemoprotein; geometric isomerization.

1. Introduction

Unsaturated fatty acids are carboxylic acid compounds in which there is at least one carbon-carbon double bond (C=C) or triple bond (C≡C) within their hydrocarbon chains [1]. These are classified into various forms based on chain length (odd and even numbers from 4 to 38 carbons), degree of unsaturation (mono-, di-, and polyunsaturated fatty acids), position of the unsaturated bond, and particularly the *cis*/*trans* configuration of the ethylene double bond. Compared to saturated fatty acids with straight structures, unsaturated fatty acids found in vegetables or fishes are typically skewed due to their double-bonded carbons in a *cis* geometric configuration [2]. Hydrogenation (*i.e.*, a chemical reaction adding hydrogens to unsaturated carbon-carbon bonds) in the presence of metal catalysts, such as nickel, palladium, or platinum, converts unsaturated fatty acids to saturated fatty acids [3]. This hydrogenation process has been applied to the food industry to convert vegetable/fish oils into semi-solidified lipids (*e.g.*, shortenings, margarines, and partially hydrogenated oils) and solidified lipids. However, the consumption of these hydrogenated lipids has been proposed to be a modern health concern because the production of industrial *trans*-fats occurs with a high probability as the result of a side reaction with the metal catalysts during the hydrogenation [4]. Unsaturated fatty acids containing only double bonds in a *trans* configuration have straight hydrocarbon chains similar to saturated fatty acids, while showing a higher risk of cardiovascular disease (almost double) than saturated fatty acids [5]. On the other hand, some kinds of naturally occurring *trans*-fatty acids have been shown to have potential nutraceutical benefits. For example, vaccenic acid ($C_{18:1}$, *trans*-Δ^{11}), which is the predominant *trans*-fatty acid found in human milk, ruminant fats, and various dairy products, has been reported to exhibit beneficial effects on health [6, 7], compared to industrial *trans*-fatty acids like elaidic acid ($C_{18:1}$, *trans*-Δ^{9}). More recently, it was revealed that vaccenic acid enhances effector $CD8^+$ T cell function and promotes anti-tumor immunity by inactivating the short-chain fatty acid receptor GPR43, demonstrating its translational potential for tumor treatment [8]. Since the human body cannot endogenously produce vaccenic acid, there has been emerging needs for the artificial synthesis of *trans*-fatty acid. In this context, food

scientists have strived to control the *cis*/*trans* isomerism of unsaturated lipids in food products [4, 9], and innovative enzymes that directly catalyze the *cis*/*trans* isomerization of unsaturated lipids has been suggested as a promising strategy [10].

A cytochrome *c*-type hemoprotein, *cis*/*trans* fatty acid isomerase (CTI) found in a few Gram-negative bacteria, including *Pseudomonas* and *Vibrio* strains [11], is the only biocatalyst that can directly catalyze the geometric isomerization of monounsaturated fatty acids. Compared to natural polyunsaturated fatty acids with conjugated double bonds in *trans* configurations, such as parinaric acid from the seeds of *Parinari laurina* [12], punicic acid from the seeds of *Punica granatum* [13], and rumenic acid from the ruminant meats and dairy products [14], *trans*-monounsaturated fatty acids have been often observed in the membrane phospholipids of *Pseudomonas* and *Vibrio* strains [15, 16], though they are mainly found in industrial lipids (unnatural) or ruminant fats (natural). Previous studies on *Pseudomonas* strains revealed that these unusual *trans*-lipids can be synthesized by CTI constitutively expressed in the bacterial periplasm [17, 18]. The CTI enzyme, as part of the short-term adaptation mechanisms in *Pseudomonas* strains, rigidifies membrane fluidity by increasing the *trans*/*cis* ratio of unsaturated fatty acid moieties in membrane phospholipids in response to environmental stressors, such as organic solvents, heat, low pH, heavy metals, and osmotic shock [19, 20]. An iron-containing heme cofactor covalently bound to the heme-binding motif can interact with the carbon-carbon double bonds in unsaturated lipids and catalyzes the *cis*/*trans* isomerization [18]. Unfortunately, only two previous studies successfully purified wild-type CTIs from *Pseudomonas* strains [21, 22], and even worse, these works used imprecise methodologies to derive data, lacking numerical catalytic information.

A strain *P. putida* KT2440, which is a Gram-negative, rod-shaped, and saprophytic soil bacterium, has become a promising workhorse for applied microbiology owing to its metabolic versatility, genetic accessibility, absence of pathogenic aspects, and stress-resistances [23, 24]. Among its unique characteristics, the short-term resistance has garnered significant attention in the field of membrane engineering, aiming to enhance robustness of bacterial strains [25]. Moreover, a complete genome sequence of

P. putida KT2440 was revealed [26], and a gene of CTI (Uniprot ID Q88KB4) is available. Notably, we investigated the periplasmic fraction of *P. putida* KT2440 for the determination of kinetic parameters of the CTI reaction using our newly established CTI reaction assay [10]. Therefore, in the present study, we purified a wild-type CTI from *P. putida* KT2440 and investigated its catalytic and structural properties. The CTI proteins were purified from the periplasmic extracts of *P. putida* KT2440 strain via serial chromatographic purification. Then, its isomerizing properties in terms of substrate specificity, optimal reaction conditions, and enzyme kinetics were determined using our CTI assay. Finally, its structural characteristics were discussed based on predicted structure models from latest computational protein structure prediction methods to understand its catalytic mechanism. The results presented here offer both theoretical and practical insights for exploring further the potential of CTI as a powerful biocatalyst for directly regulating the geometric isomerization of dietary monounsaturated fatty acids.

2. Materials & Methods

2.1. Materials

Methyl palmitoleate (≥95.0%), palmitoleic acid (≥98.0%), and chloramphenicol (≥98.0%) were purchased from Tokyo Chemical Industry Co. (Chuo-ku, Tokyo, Japan). Methyl palmitelaidate (≥98.0%) and palmitelaidic acid (≥99.0%) were purchased from Santa Cruz Biotechnology Co. (Santa Cruz, CA, USA). Bis(2-ethylhexyl) sulfosuccinate sodium salt (AOT, ≥97.0%), methyl oleate (≥98.5%), methyl elaidate (≥99.0%), *cis*-11-vaccenic methyl ester (≥95.0%), *trans*-11-vaccenic methyl ester (≥95.0%), *cis*-vaccenic acid (≥97.0%), and vaccenic acid (≥99.0%) were purchased from Sigma-Aldrich Co. (St. Louis, MO, USA). Oleic acid (≥99.0%), elaidic acid (≥98.0%), and lysozyme (20,000 units/mg) were purchased from Thermo Fisher Scientific Co. (Waltham, MA, USA). Gas chromatography (GC)-grade organic solvents and other chemicals (guaranteed reagent grade) were purchased from Daejung Chemicals & Metals Co. (Siheung, Gyeonggi-do, Republic of Korea).

2.2. Bacterial strain and culture conditions

A gram-negative strain of *Pseudomonas putida* KT2440 (ATCC® 47054™) was acquired from the American Type Culture Collection (Manassas, VA, USA), and cultured following the manufacturer's instruction. The cells were inoculated in 5 mL of LB broth with 20 μg/mL chloramphenicol and cultivated at 37℃ and 220 rpm for 16 h (pre-culture). Notably, an antibiotic supplement was used to control contamination by other bacteria because this *Pseudomonas* strain is known to be resistant to multiple antibiotics, especially chloramphenicol [27]. The cultured cells (1:100, v/v) were subsequently inoculated in 2 L Erlenmeyer flasks containing 500 mL of LB broth with 20 μg/mL chloramphenicol. Then, the cultures were incubated at 37℃ and 220 rpm until the optical density (OD_{600}) reached 1.6 (approximately 24 h). These cells were harvested via centrifugation (4,000 *g*, 20 min, 4℃), and the harvested cells were stored at –80°C until further use.

2.3. Formation of spheroplasts and periplasmic extraction

The collected *P. putida* KT2440 cells were converted to spheroplasts, and their periplasmic fractions were extracted as previously described [10, 22] with slight modifications. Dried cells (20 g) resuspended in 250 mL of buffer A (100 mM Tris-HCl, 20%(w/v) sucrose, pH 8.0) were incubated at 4℃ for 5 min, and then, 250 mL of buffer B (100 mM Tris-HCl, 20%(w/v) sucrose, 5 mM EDTA, pH 8.0) as well as 20 mg of lysozyme were added. The resulting cell suspensions (final 500 mL) containing 100 mM Tris-HCl (pH 8.0), 20%(w/v) sucrose, 2.5 mM EDTA, and 40 μg/mL lysozyme were stored at 4℃ for 25 min with continuous mechanical stirring (350 rpm). By centrifugation (4,000 *g*, 20 min, 4℃), the spheroplasts were separated, and the clear supernatants were collected to be utilized as crude periplasmic fractions for the subsequent protein purification process.

2.4. Serial chromatographic purification of CTI

Protein purification based on serial chromatography was performed as previously described [28, 29]

with slight modifications. Crude periplasmic extracts (500 mL) were mixed with 183 g of ammonium sulfate (60% saturation) with 12%(w/v) increments at 4℃ with continuous stirring (350 rpm) in order to precipitate crude protein extracts with CTI activity, and after 1 h of incubation, the suspensions were fractionated by centrifugation (4,000 *g*, 20 min, 4℃). The resulting precipitates were dissolved in 10 mL of 20 mM Tris-HCl buffer (pH 8.5) and dialyzed overnight into the same buffer using a 12 kDa MWCO dialysis sack. The resulting dialysates were concentrated using a 50 kDa MWCO centrifugal filter and subjected to further serial chromatographic purification process via an ÄKTA go™ fast protein liquid chromatography (FPLC) system (Cytiva Co., Marlborough, MA, USA) equipped with an ultraviolet (UV) detector (Cytiva Co.) to measure the absorbance at 280 nm wavelength. The protein samples were sterile filtered through a 0.45 μm cellulose acetate filter before injection. First of all, the crude proteins obtained from 60%(w/v) ammonium sulfate precipitation were loaded onto a 1 mL HiTrap® Q Fast Flow (FF) anion exchange chromatography column (Cytiva Co.) equilibrated with 20 mM Tris-HCl buffer (pH 8.5), and proteins were eluted with a gradient of sodium chloride (NaCl, 0.0–0.5 M) at a flow rate of 1.0 mL/min. Second, the protein fractions exhibiting CTI activity were collected, sufficiently concentrated by ultrafiltration (50 kDa MWCO), and loaded onto a 1 mL HiTrap® DEAE FF anion exchange chromatography column (Cytiva Co.) equilibrated with 20 mM Tris-HCl buffer (pH 8.5). The elution was conducted as described above. Lastly, the protein fractions exhibiting CTI activity were collected, dialyzed into 50 mM potassium phosphate buffer (pH 7.2) containing 0.15 M NaCl, sufficiently concentrated by ultrafiltration (50 kDa MWCO), and loaded onto a 120 mL HiPrep™ 16/60 Sephacryl® S-100 HR size exclusion chromatography column (Cytiva Co.) equilibrated with 50 mM potassium phosphate buffer (pH 7.5) containing 0.15 M NaCl. The proteins were eluted at a flow rate of 0.5 mL/min. The protein fractions showing CTI activity were collected, dialyzed into 50 mM potassium phosphate buffer (pH 7.5), concentrated by ultrafiltration, and stored at refrigeration temperature before reactions. The purity was determined by SDS-PAGE analysis, and concentration was measured by the Bradford method. All purification steps were carried out at 4℃.

151

152 *2.5. Enzyme activity assays for CTI*

153 The catalytic activity of CTI was measured in two different ways – aqueous buffer solution system
154 and reversed micelle system [10] – based on the experimental purpose. For the activity screening dur-
155 ing the purification, the catalytic activity of CTI was determined in the modified aqueous buffer solu-
156 tion reaction system. Each protein fraction (dissolved in 50 mM potassium phosphate buffer, pH 7.5)
157 was used as the reaction medium. The reaction mixture (approximately 0.9 mL) was incubated for 10
158 min in a 5 mL glass vial within a water bath set at 25°C and 800 rpm. The CTI reaction was initiated
159 upon addition of substrate (10 mM) to achieve a total volume of 1 mL, followed by a brief vortexing.
160 At the end of the reaction (for 1 h), the reaction mixtures were transferred to a microcentrifuge tube,
161 vortexed with 1 mL of isooctane for 20 sec, and then centrifuged (14,000 *g*, 5 min) to separate the
162 organic layer containing hydrophobic substrates and products (the vortex-centrifugation steps were
163 repeated if phase separation was not achieved). The organic layer (0.8 mL) was obtained, and the
164 solvent was evaporated at room temperature via a nitrogen evaporator (MGS-3100; Eyela Co., Bohe-
165 mia, NY, USA). The dried samples were stored at −18°C before further analysis. For the investigation
166 of catalytic properties, the catalytic activity was determined in the reversed micelle reaction system.
167 The enzyme solutions (0.09 mL, dissolved in 50 mM potassium phosphate buffer, pH 7.5) were added
168 to 4.41 mL of 113.38 mM AOT/isooctane, sufficiently vortexed to generate reversed micelles (visually
169 clear), and pre-incubated at 25°C and 800 rpm for 10 min. By adding 0.5 mL of substrates (dissolved
170 in isooctane) at each molar concentration, the reactions were initiated, and 0.3 mL of aliquots were
171 sampled at a specific reaction time. The same evaporation and storage processes were conducted as
172 described above. The calculation for the conversion rate (%) from *cis* configuration to *trans* configu-
173 ration was performed as follows:

174 $$Conversion\ rate\ (\%) = \frac{[trans]_t}{[cis]_t + [trans]_t} \times 100$$

where $[cis]_t$ and $[trans]_t$ are the amounts of unsaturated fatty acids in *cis* and *trans* configurations at each specific reaction time *t*, respectively. For the kinetics of CTI reaction, all reactions were analyzed according to the Michaelis-Menten assumption using SigmaPlot software (ver. 12.5; Systat Software Co., San Jose, CA, USA). The kinetic parameters were derived by computational non-linear regression analysis, and the relevant assumption was validated by double-reciprocal plotting as follows:

$$\frac{[S]}{v} = \frac{1}{V_{max}} \times [S] + \frac{K_m}{V_{max}}$$

where $[S]$ is the concentration of substrate, v is the initial velocity of the reaction, V_{max} is the maximum initial velocity, and K_m is the dissociation constant of the enzyme-substrate complex. One unit (U) was defined as the amount of enzymes converting 1 μmol of substrates to products per minute.

2.6. Fatty acid methylation and gas chromatography analysis

Unsaturated fatty acids in the dried reaction mixture were methylated using Fatty Acid Methylation Kit (Nacalai Tesque Co., Nakagyo-ku, Kyoto, Japan) as previously described [10]. The dried samples were fully dissolved in 0.5 mL of reagent A (a mixture of toluene/methanol in a ratio of 52:48, v/v), followed by vortexing with 0.5 mL of reagent C (a strong acidic BF_3-methanol solution). Subsequently, the mixture was incubated at 37°C for 20 minutes to catalyze the methylation of free fatty acids. After extracting formed fatty acid methyl esters with 1 mL of *n*-hexane, the *n*-hexane layers were rinsed with deionized water, filtered through a 0.45 μm polytetrafluoroethylene syringe filter, transferred into autosampler vials with vial inserts for GC analysis, and analyzed using a YL6500 GC system (Young In Chromass Co., Anyang, Gyeonggi-do, Republic of Korea) equipped with a flame ionization detector (FID) and a cyanopropyl phase DB-FastFAME capillary column (30 m × 0.25 mm × 0.25 μm; Agilent Technologies Co., Santa Clara, CA, USA). Helium (≥99.999%) was employed as the carrier gas at a constant flow rate of 1.0 mL/min. One microliter of the sample was injected into a split flow configuration at a ratio of 50:1(v/v), and other operating details are summarized in Supplementary Data Table

S1. Calibration curves for monounsaturated fatty acid methyl esters under the aqueous buffer solution reaction condition were derived in this study (Supplementary Data Fig. S2), and for the reversed micelle condition, calibration curves were adapted from our previous studies [10].

2.7. Nuclear magnetic resonance (NMR) spectroscopy

Liquid-state ^{1}H NMR spectroscopy was conducted using an AVANCE™ 600 MHz high-resolution NMR spectrometer (Bruker Co., Bremen, Germany). The samples were homogeneously dissolved in dimethyl sulfoxide-d_6 with 0.03%(v/v) tetramethylsilane (TMS) as an internal standard for calibrating chemical shift. The sample observation frequency was 600.13 MHz, and the spectral width was determined to be 12 kHz. All the analyses were conducted at room temperature. The NMR data were processed using TopSpin™ software (ver. 4.0.6; Bruker Co.), and chemical shifts (δ) of each signal were given in parts per million (ppm) relative to TMS.

2.8. Computational analysis of protein structure

A complete genome sequence of *P. putida* KT2440 was distributed from ATCC, and a putative CTI gene (Uniprot ID Q88KB4) encoded in the genomic DNA was identified using nucleotide Basic Local Alignment Search Tool (https://blast.ncbi.nlm.nih.gov/Blast.cgi/). The translated amino acid sequence (Supplementary Data Fig. S3) of the putative CTI gene was used for computational prediction of the protein structure. The presence of signal peptide and the location of cleavage site were predicted using SignalP 5.0 software (https://services.healthtech.dtu.dk/services/SignalP-5.0/), which is a deep neural network-based prediction architecture for signal peptide [30]. The probabilities of signal peptide occurrence at individual amino acids were represented as regional probabilities. The three-dimensional (3D) structure was predicted utilizing RoseTTAFold software (https://robetta.bakerlab.org/). This software employs a prediction architecture featuring a deep neural network that learns relationships within and between amino acid sequences, distances, and coordinates in the protein structure [31]. Angstrom

error estimates per amino acid were calculated using DeepAccNet framework, and the confidence (1.0 good, 0.0 bad) was calculated from the local distance difference test (lDDT) score. The final predicted structure model was visualized using both PyMOL software (https://pymol.org/2/) and UCSF Chimera software (https://www.cgl.ucsf.edu/chimera/) [32].

2.9. Statistical analysis

Statistical analysis in this study was performed using SPSS statistics software (ver. 28.0; IBM Co., Armonk, NY, USA). The experimental data underwent one-way analysis of variance (ANOVA), and the statistical significance was confirmed using Duncan's multiple range test ($p<0.05$).

3. Results & Discussions

3.1. Purification of CTI proteins from P. putida KT2440

Conversion of unsaturated *cis* fatty acids to *trans*-fatty acids in membrane phospholipids of *P. putida* is brought about through the *cis*/*trans* isomerization catalyzed by CTI in the periplasm [33]. Since CTI is a cytochrome *c*-type hemoprotein, which is covalently bound with a heme C cofactor, it is translocated to the periplasm after post-translational cytochrome *c* maturation in the membrane [34]. To obtain a periplasmic fraction from *P. putida* KT2440, intact spheroplasts were formed using a hypertonic Tris-sucrose-EDTA solution, and the periplasmic fraction was separated from the spheroplast suspension by gravitational force. The periplasmic fraction of *P. putida* KT2440 cells exhibited CTI activity against palmitoleic acid, and it was used as a crude extract for the further purification of CTI proteins. Crude protein extracts were obtained from the periplasmic fraction by 60%(w/v) ammonium sulfate precipitation, while 60–100%(w/v) precipitates exhibited no CTI activity. From these crude extracts, the CTI protein was purified through a chromatographic purification process (Fig. 1). Comprehensive results of the CTI purification are summarized in Table 1, and at the final step, the purified CTI proteins were obtained with a 110.07 purification fold, 2.07% recovery, and 351.94 mU/mg specific activity.

Compared to previous purifications from *P. oleovorans* GPo12 (3.6 U/mg) [22] and *P. psychrophila* (0.63 U/mg) [21], the isolation productivity from *P. putida* KT2440 was relatively lower (0.35 U/mg from 80 g cells). This difference might be attributed to slight discrepancies in spheroplasting efficiency, antibiotic usage, or assay, although CTI proteins were isolated from *P. putida* KT2440 without destabilizing proteins or sacrificing activity.

During anion exchange chromatography, the CTI proteins failed to bind to either strong (Fig. 1a) or weak (Fig. 1b) anion exchangers equilibrated with 20 mM Tris-HCl buffer (pH 8.5). Unbound protein fractions (0 M sodium chloride) exhibited CTI activity, whereas no CTI activity was detected in any eluted fractions of anion exchange chromatography processes. This phenomenon has been observed in previous studies of CTIs from other *Pseudomonas* strains [21, 22]. Cytochrome *c*-type proteins generally exhibit high isoelectric points within a basic pH range (9.0–11.0), resulting in a positive net charge within a neutral pH range [35]. We used this charge state for removing other protein contaminates that were adsorbed to the ion exchangers during anion exchange chromatography (Fig. 1a–b). After sufficient fractionation, the unbound fractions were directly applied to size exclusion chromatography (Fig. 1c). Proteins with CTI activity were eluted at 44–51 mL elution volumes (0.5 mL/fraction), peaked at 46 mL elution volumes, and the ratio of elution volume to void volume (V_e/V_o) at the peak was 1.861. Based on these results, the molecular weight of CTI was calculated to be approximately 85 kDa using the calibration curve of analytical size exclusion chromatography (Fig. 2a). The SDS-PAGE analysis revealed a protein band within the eluted fractions, ranging between 75 kDa and 100 kDa, thereby confirming the molecular weight of the purified CTI (Fig. 2b). Considering a signal peptide-truncated N-terminus and its monomeric structure, the theoretical molecular weight (approximately 85 kDa) of CTI corresponds to the observed molecular weight. Other wild-type CTIs purified from different *Pseudomonas* strains have been reported to show 80 kDa molecular weights [21, 22], indicating shared conserved genes and protein structures.

3.2. Catalytic properties of the purified CTI from P. putida KT2440

The periplasmic CTI enzyme targets the unsaturated fatty acid moieties of membrane phospholipids; however, the purified CTI enzyme isolated from the periplasm catalyzes the *cis*/*trans* isomerization of monounsaturated fatty acids under *in vitro* conditions [21, 22]. To confirm substrate preference against dietary monounsaturated fatty acids, which exist predominantly in food products: oleic acid ($C_{18:1}$, *cis*-Δ^9), *cis*-vaccenic acid ($C_{18:1}$, *cis*-Δ^{11}), and palmitoleic acid ($C_{16:1}$, *cis*-Δ^9), time-dependent reactions of wild-type CTI purified from *P. putida* KT2440 against them were conducted until reaction equilibration (Fig. 3). Focusing primarily on the reaction involving palmitoleic acid, before the reaction, only the peak (at 6.68 min) corresponding to methyl palmitoleate was detected, whereas this peak decreased (approximately 25%) and a new peak (at 6.58 min) corresponding to methyl palmitelaidate proportionally increased after the 30 min reaction (Fig. 3a). Each *trans* isomers of all monounsaturated fatty acid substrates were liberated at the early stage of the CTI reaction, and their methyl esters were detected before their *cis* isomers with a high-resolution factor in the GC-FID analysis, with a standard deviation of retention time less than 1% (Supplementary Data Table. S4). Notably, while CTI showed a somewhat promiscuity, a strong substrate specificity on palmitoleic acid was observed (Fig. 3b). The calculated conversion rate for palmitoleic acid reached 98.74% ± 1.04%, while for *cis*-vaccenic acid and oleic acid, it amounted to 54.06% ± 4.06% and 17.09% ± 0.56%, respectively (Fig. 3c). It has been reported that wild-type CTIs purified from *Pseudomonas* might adopt palmitoleic acid as its major substrate because the monounsaturated acyl moiety of membrane phospholipids is primarily composed of palmitoleic acid (major) and *cis*-vaccenic acid (minor) [36]. Compared to other CTIs, wild-type CTI purified from *P. putida* KT2440 acted on both *cis*-vaccenic acid and oleic acid, indicating its substrate promiscuity for unsaturated fatty acids with chain lengths and double bond positions. Additionally, ^{1}H NMR spectroscopy on the CTI reaction products against palmitoleic acid showed that only a minor shift in the splitting patterns of hydrogen atoms on the ethylene double bond was observed, while other splitting patterns remain unchanged (Supplementary Data Fig. S5), indicating that only the *cis*/*trans*

isomerization reaction occurred. In other words, these results demonstrate that only geometric isomers of palmitoleic acid were in the reactants, with no other compounds produced.

The main dietary source of *trans*-fats is elaidic acid ($C_{18:1}$, *trans*-Δ^9), which is produced during the hydrogenation of vegetable oils containing oleic acid ($C_{18:1}$, *cis*-Δ^9) and linoleic acid ($C_{18:2}$, *cis*-$\Delta^{9,12}$). However, in practice, numerous types of *trans*-fatty acids are found in both natural and processed food products, depending on the number and position of double bonds, and the length of their alkyl moieties [37]. Among them, palmitelaidic acid ($C_{16:1}$, *trans*-Δ^9) and vaccenic acid ($C_{18:1}$, *trans*-Δ^{11}) predominantly exist in ruminant milk fats [38]. It is crucial to find a specialized biocatalyst for controlling each different *trans*-fatty acid in food products. Therefore, the CTI purified from *P. putida* KT2440 emerges as a biocatalyst suitable for such applications. Its inherent capability to catalyze the isomerization of *cis*-fatty acids into their *trans* configurations reflects its original catalytic mechanism within the bacterial periplasm. Moreover, geometric isomerization by CTI might be a reversible reaction but biased towards the forward reaction depending on the thermodynamic stability of the enzyme-substrate complex [39], suggesting further evolution to regulate the isomerism in a desired direction. Of course, in a current form, CTI can serve as a valuable resource for producing *trans*-fatty acids, especially vaccenic acid, and various *cis*/*trans* mixtures for research purposes. There has been no approach to making them under eco-friendly conditions [39, 40].

Finally, focusing on a primary substrate, palmitoleic acid, the impact of various physicochemical conditions on the catalytic activity of wild-type CTI purified from *P. putida* KT2440 was assessed to ascertain its optimal conditions. In the case of pH, a typical bell-shaped curve was observed within the range of pH 5.0–10.0, and it peaked in the neutral pH range of 7.0–7.5 (Supplementary Data Fig. S6a). In the case of reaction temperature, the activity of CTI was highest at 25℃ (Supplementary Data Fig. S6b). Compared with the recombinant CTI [41], the current findings are closer to originality, indicating that slight structural differences can lead to catalytic deviations. When exposed to harsh conditions, CTI retained over 50% of its activity at low temperatures (5–10℃) but showed a dramatic decrease in

activity at high temperatures (45–60℃). Some cytochrome *c*-type proteins act as cold-active enzymes, which are active at lower temperatures but sensitive at higher temperatures [42]. The optimal reaction conditions for wild-type CTI from *P. putida* KT2440 were determined to be at pH 7.5 and 25℃ against palmitoleic acid. Its physicochemical stability under storage at different pH (2.0–11.0) or temperatures (5–60℃) were also evaluated (Supplementary Data Fig. S7). It was somewhat unstable at acidic pH values (below 5.0) and at high temperatures (above 50℃), indicating that, for industrial applications, identifying the amino acid residues that enhance either thermal or pH stability would be crucial.

3.3. Enzyme kinetics of the purified CTI from P. putida KT2440

Under optimal reaction conditions (25℃ and pH 7.5), exploratory kinetic parameters of the purified CTI from *P. putida* KT2440 were assessed against palmitoleic acid (Fig. 4) using our reversed micelle reaction system that facilitates the precise and reproducible observation of time-resolved CTI reactions [10]. The initial velocity (v) at the early stage (0–30 min) increased as substrate concentration (0.10–1.20 mM) increased and became saturated above 0.6 mM palmitoleic acid (Fig. 4a), following a typical Michaelis-Menten kinetic model of the single-substrate reaction. The kinetic parameters of V_{max} and K_m were determined to be 0.028 mM·min^{-1} and 0.277 mM, respectively. The Michaelis-Menten kinetic assumption and parameters were validated by double-reciprocal plotting (Fig. 4b). Under the assumption of the molecular weight of the CTI enzyme, its turnover number (k_{cat}) was 0.14 sec^{-1}, and catalytic efficiency (k_{cat}/K_m) was consequently calculated as 5.13×10^2 M^{-1}·sec^{-1}. Notably, the substrate affinity ($1/K_m$) toward palmitoleic acid (3.61 mM^{-1}) was 2.5-fold higher than that toward oleic acid (1.47 mM^{-1}) [10]. This significant discrepancy in the dissociation constant (K_m) suggests that the substrate specificity of CTI exhibits slight promiscuity toward monounsaturated fatty acids. In contrast, their similar turnover numbers (k_{cat}) indicate that once substrates bind at the active site, its *trans* isomer is liberated at an analogous rate independent of the structure, indicating that the rate-determining step is the access and binding of the substrate. In the case of the same CTI family [21], catalytic efficiency of the purified

CTI enzyme from *Pseudomonas* sp. strain E-3 can be theoretically calculated as 4.31×10^3 $M^{-1} \cdot sec^{-1}$ considering the given information, which is slightly higher than wildtype CTI from *P. putida* KT2440. Nevertheless, its substrate promiscuity is a valuable aspect for further adaptation to various monounsaturated fatty acids and control over their *cis*/*trans* isomerism.

Not fully understood, cytochrome *c*-type CTIs directly interact with monounsaturated fatty acids at the active site and catalyzes geometric isomerization without chemical support and energy input [43]. In a kinetic pattern (Fig. 4a), there was no evidence of allostericity, cooperativity, or substrate/product inhibition. Enzymes within the same *cis*/*trans* isomerase family (EC 5.2.), such as linoleate isomerase (EC 5.2.1.5) and enoyl-CoA-(Δ) isomerase (EC 5.3.3.8), also catalyze the geometric isomerization of unsaturated fatty acids. Since these enzymes typically involve complicated catalysis steps, undesired side reactions (*e.g.*, the transposition of double bonds), other chemical/enzymatic assistances, and strict substrate specificities, it is challenging to use them for industrial purposes as standalone catalysts to produce a desired compound. During the reaction, the total amounts of *cis* and *trans* isomers remained constant, and unidentified acyl intermediates and byproducts were not detected. Therefore, these findings demonstrate that CTI purified from *P. putida* KT2440 catalyzes the direct isomerization of monounsaturated fatty acids without requiring other reactions or chemical assistance. Other wild-type CTIs from different *Pseudomonas* strains showed similar kinetic properties [21, 22], indicating that these enzymes might share the same mechanism for catalysis based on the conserved cytochrome *c* domains. In the case of other cytochrome *c*-type proteins, there is no reports about their biochemical activity on the monounsaturated fatty acids. Therefore, it should be considered that the CTI enzyme can belong to the family of *cis*/*trans* isomerases (EC 5.2.) as a novel classification of biocatalysts that isomerize the *cis*/*trans* (geometric) configuration of each specific monounsaturated fatty acid.

3.4. Structural properties of the purified CTI from P. putida KT2440

In order to understand the catalytic mechanism of wild-type CTI from *P. putida* KT2440, its protein

structural properties were investigated using deep learning-based protein structure predictions (Fig. 5). The mature CTI protein is a large polypeptide consisting of 766 amino acids (Fig. 5a) compared with other cytochrome *c*-type hemoproteins (~20 kDa). Predictions revealed that CTI is composed of three separate domains. The CTI apoprotein has a signal peptide at its N-terminus (Fig. 5b), which is typically found at the N-terminals of other apocytochromes. A leader sequence from the 1st to 20th amino acid residues (MVHRILAGAFAKKOSGAVFG) is recognized by the Sec-dependent secretory pathway in Gram-negative bacteria, and by signal peptidase I, its cleavage occurs right after the 20th amino acid. To respond to environmental changes and the subsequent efflux of cytoplasmic components, CTIs and other protective enzymes should be located in the periplasm. Signal peptides present at their N-terminals function to translocate them into the bacterial periplasm after translation. The observed molecular weight of CTI was approximately 85 kDa in its purified state, indicating the presence of a signal peptide that might be removed during membrane translocation. A signal sequence of wild-type CTI from *P. putida* KT2440 is conserved with other CTI genes found in the same genus of *Pseudomonas* [33], and this sequence appears to be compatible with other Gram-negative bacteria, like *Escherichia coli* [25]. When the CTI gene is heterologously expressed in *E. coli* strain, it is unnecessary to substitute its native signal sequence for others. Of course, membrane translocation mediated by signal sequence does not ensure proper folding of the CTI protein due to its cytochrome nature.

Then, a protein 3D structure model for wild-type CTI from *P. putida* KT2440 was predicted (Fig. 5c) using its amino acid sequence (Supplementary Data Fig. S3). Considering membrane translocation, predictions were performed without an N-terminal signal peptide region (1–20 amino acid residues). Structure models were generated for the truncated CTI comprising a total of 746 amino acids, and the most optimal model was chosen. The estimated confidence for the selected model was 0.79, indicating a high accuracy of prediction, and the angstrom error estimates ranged from 0.66 to 10.04 Å (Supplementary Data Fig. S8). The angstrom errors for most amino acid residues were below 4.00 Å, whereas the prediction of the first five amino acids (QAPQS, signal peptide-cleaved loop region) was imprecise.

Calculating the folding of the truncated region after cleavage remains a challenge. Nevertheless, the model represented two structural features: a cytochrome *c* domain and another repetitive bulky domain.

The CTI enzyme derived from *P. putida* KT2440 possesses one heme-binding motif (CVACH, 43–47 amino acid residues). Prediction showed that its cytochrome *c* domain (21–180 amino acid residues) is similar to other monoheme cytochromes *c*, which consist of several α-helices, additional loops, one heme-binding motif, and one heme C cofactor (Fig. 5c). One heme C with an iron ion was artificially aligned near the predicted heme-binding motif of CTI. Indeed, the formation of cytochrome *c* entails the establishment of thioether bonds linking the vinyl groups of heme C molecule with the thiol groups of the heme-binding motif [34]. Considering this, two cysteine thiol groups (Cys_{43} and Cys_{46}) of the heme-binding motif covalently bind to the vinyl groups of the heme C. One of the axial coordination sites of the iron ion within heme C can be bound to a nitrogen atom belonging to the proximal histidine (His_{47}) in the heme-binding motif, forming a pentacoordinated octahedral complex. This coordination complex enables CTI to perform electron transfer as the catalytic center, and its catalytic significance for the geometric isomerization was proposed by a mutagenesis study [18]. The carbon-carbon double bond of monounsaturated fatty acids can bind with a heme C via coordination at the distal axial ligand position [44], which results in a hexacoordinated octahedral complex. Based on this predicted structure of the putative catalytic domain, the binding pocket surrounding the heme-binding motif was analyzed, along with the substrate alignment (Fig. 6). The binding pocket of the catalytic domain of CTI, which predominantly consists of hydrophobic amino acids, is predicted to be directly exposed to the external surface and has a space with straight-line dimensions ranging from 20−23 Å. Monounsaturated fatty acids with a hydrophobic chain are accessible into the hydrophobic binding pocket, where the ethylene double bond interacts with an iron ion of the heme *c* cofactor. For effective *cis*/*trans* isomerization, the ethylene double bond of monounsaturated fatty acids should be precisely positioned at the heme center. Linked to the substrate preference of CTI, the double bond of palmitoleic acid in the ω-7 position (~8.6 Å terminal length) can be properly aligned at the center of the heme *c* cofactor, whereas that of oleic

424 acid in the ω-9 position (~12.7 Å terminal length) is expected to be loosely-fitted due to its elongated
425 length, causing a shift forward of the double bond. In the case of *cis*-vaccenic acid, it exhibited three
426 times higher CTI activity than oleic acid despite having the same alkyl chain ($C_{18:1}$) but it has a double
427 bond in the ω-7 position, which is suitable for the CTI reaction, similar to palmitoleic acid. Additionally,
428 CTI exhibited higher substrate specificity against palmitoleic acid than against *cis*-vaccenic acid, prob-
429 ably because molecular interactions between the carboxyl group of fatty acids and hydrophilic amino
430 acids of CTI, such as electrostatic interaction and dipole-dipole attraction, at the entrance of the binding
431 pocket help stabilize the enzyme-substrate complex. The substrate specificity of wildtype CTI is there-
432 fore based on the alkyl chain length and the double bond position of the substrates. Thus, the structure
433 of CTI may have evolved to be suited for 9-hexadecenoic acid, while its promiscuity can be explained
434 by the loose binding entrance and large heme-binding pocket. When bound to the heme iron, π-orbitals
435 of the double bond of monounsaturated fatty acids are highly susceptible to electron donation to the
436 iron in the ferric (Fe^{3+}) state [45]. Not still fully understood, the removal of an electron from the double
437 bond transforms a non-rotated double bond (sp^2) to a freely rotated state (sp^3) without transient satu-
438 ration [43]. Consequently, when the enzyme-substrate complex dissociates, the carbon-carbon double
439 bond can be spontaneously reconstituted depending on its thermodynamic stability [39].
440 Finally, the mature cytochrome *c*-type CTI from *P. putida* KT2440 has a very long primary protein
441 structure consisting of a chain of 746 amino acids, compared to other small monoheme cytochrome *c*-
442 type (class I) hemoproteins. The prediction showed that the other protein domain (181–766 amino acid
443 residues) after the cytochrome *c* domain forms a parasol-like polypeptide chain with repetitive bulky
444 structures (Fig. 5c). This peculiar domain, composing three analogous segments featuring a single β-
445 sheet and extended α-helices, is distinguished from the catalytic domain. Notably, no conserved motif
446 related to cytochromes *c* or other catalysts was identified in the structure, indicating that it has no direct
447 association with catalytic properties. On the other hand, from the architectural perspective, a group of
448 long α-helices distributed in random directions totally envelops the cytochrome *c* domain, and three

similar β-sheets appear to stabilize the structure. This parasol-like architecture suggests that when the bacterial membrane is exposed to external harsh conditions the periplasmic CTI protein partially spans the damaged membrane through its parasol-like transmembrane domain, which allows its cytochrome *c* domain to penetrate to an appropriate depth for the geometric isomerization of phospholipids. This demonstration corresponds to the proposed *in vivo* mode of action of CTI [46]. The CTI hemoprotein with an additional parasol-like transmembrane domain is considered to have an advantage for practical applications in the food and lipid industry where hydrophilic enzymes face challenges accessing hydrophobic substrates in real food products containing oils and fats. Of course, CTI did not catalyze the *cis*/*trans* isomerization of palmitoleic acid in a triacylglycerol form, tripalmitolein, probably due to difficulty in accessing the heme-binding site. Therefore, for future applications of CTI in food products, its structure should be artificially modified to allow the use of triacylglycerols as substrates.

4. Conclusions

In the present study, a cytochrome *c*-type CTI was isolated from the periplasmic fraction of *P. putida* KT2440 through serial chromatographic purification. This large, monomeric CTI protein catalyzed the *cis*/*trans* isomerization of the double bond in dietary monounsaturated fatty acids. These results suggest that the CTI enzyme belongs to the family of *cis*/*trans* isomerases (EC 5.2.) as a novel classification of biocatalysts, which require neither ATP nor cofactors. Moreover, structural understanding of CTI revealed its monoheme cytochrome *c* domain covered with a parasol-like transmembrane domain. These findings shed light on the catalytic mechanism of CTI, as well as its potential as an industrial biocatalyst for controlling the *cis*/*trans* isomerism of monounsaturated fatty acids. The exploration in this study, which found simple kinetics, robustness, and promiscuity of CTI from *P. putida* KT2440, suggest its potential for repurposing in industrial applications as a biocatalyst to directly control geometric isomerism of monounsaturated fatty acids found in food products. For the practical application of CTI, further studies should focus on mass production platform, stability enhancement, specificity

diversification, and immobilization of CTI via biotechnological approaches. Especially, further protein engineering of the catalytic domain can evolve CTI to have each different substrate specificity on various monounsaturated fatty acids, as well as triacylglycerols found in dietary lipids.

CRediT Authorship Contribution Statement

Jun-Young Park: Conceptualization, Investigation, Data curation, Writing - Original draft, Writing - Review & Editing, Visualization. **Min-Gyeong Lee**: Investigation, Validation, Formal analysis, Visualization, Writing - Review & Editing. **Dimitris Charalampopoulos**: Writing - Review & Editing. **Kyung-Min Park**: Writing - Review & Editing, Project administration, Funding acquisition. **Pahn-Shick Chang**: Conceptualization, Writing - Review & Editing, Supervision, Project administration.

Declaration of Competing Interest

The authors declare that they have no known competing financial interests or personal relationships that could have appeared to influence the work reported in this paper.

Data Availability

Data will be made available on request.

Acknowledgments

This work was carried out with the supports of the National Research Foundation of Korea (NRF) grant funded by the Korea government (MSIT) (No. 2020R1C1C1009678) and "Cooperative Research Program for Agriculture Science & Technology Development (Project No. PJ01488802)" provided by Rural Development Administration, Republic of Korea.

References

[1] Y. Liu, N. Shen, H. Xin, L. Yu, Q. Xu, Y. Cui, Unsaturated fatty acids in natural edible resources, a systematic review of classification, resources, biosynthesis, biological activities and application, Food Bioscience 53 (2023) 102790.

[2] A.-B. Oteng, S. Kersten, Mechanisms of action of *trans* fatty acids, Advances in Nutrition 11(3) (2020) 697-708.

[3] M.K. Gupta, Chapter 7 - Hydrogenation, in: M.K. Gupta (Ed.), Practical guide to vegetable oil processing (Second edition), AOCS Press2017, pp. 171-215.

[4] D.R. Kodali, 1 - *Trans* fats: Health, chemistry, functionality, and potential replacement solutions, in: D.R. Kodali (Ed.), Trans fats replacement solutions, AOCS Press2014, pp. 1-39.

[5] D. Mozaffarian, A. Aro, W.C. Willett, Health effects of *trans*-fatty acids: experimental and observational evidence, European Journal of Clinical Nutrition 63(2) (2009) 5-21.

[6] C.M.C. Bassett, A.L. Edel, A.F. Patenaude, R.S. McCullough, D.P. Blackwood, P.Y. Chouinard, P. Paquin, B. Lamarche, G.N. Pierce, Dietary vaccenic acid has antiatherogenic effects in $LDLr^{-/-}$ mice, The Journal of Nutrition 140(1) (2010) 18-24.

[7] Y. Wang, M.M. Jacome-Sosa, D.F. Vine, S.D. Proctor, Beneficial effects of vaccenic acid on postprandial lipid metabolism and dyslipidemia: Impact of natural *trans*-fats to improve CVD risk, Lipid Technology 22(5) (2010) 103-106.

[8] H. Fan, S. Xia, J. Xiang, Y. Li, M.O. Ross, S.A. Lim, F. Yang, J. Tu, L. Xie, U. Dougherty, F.Q. Zhang, Z. Zheng, R. Zhang, R. Wu, L. Dong, R. Su, X. Chen, T. Althaus, P.A. Riedell, P.B. Jonker, A. Muir, G.B. Lesinski, S. Rafiq, M.V. Dhodapkar, W. Stock, O. Odenike, A.A. Patel, J. Opferman, T. Tsuji, J. Matsuzaki, H. Shah, B. Faubert, S.E. Elf, B. Layden, B.M. Bissonnette, Y.-Y. He, J. Kline, H. Mao, K. Odunsi, X. Gao, H. Chi, C. He, J. Chen, *Trans*-vaccenic acid reprograms $CD8^+$ T cells and anti-tumour immunity, Nature 623(7989) (2023) 1034-1043.

[9] T.A. Ghebreyesus, T.R. Frieden, REPLACE: A roadmap to make the world *trans* fat free by 2023,

524 The Lancet 391(10134) (2018) 1978-1980.
525 [10] J.-Y. Park, H.-W. Choi, K.-M. Park, P.-S. Chang, An improved method for rapid evaluation of
526 enzymatic *cis*/*trans* isomerization of C18:1 monounsaturated fatty acids, Food Chemistry 404 (2023)
527 134618.
528 [11] H.J. Heipieper, F. Meinhardt, A. Segura, The *cis–trans* isomerase of unsaturated fatty acids in
529 *Pseudomonas* and *Vibrio*: Biochemistry, molecular biology and physiological function of a unique
530 stress adaptive mechanism, FEMS Microbiology Letters 229(1) (2003) 1-7.
531 [12] R. Puri, A.K. Choudhary, P. Barman, G. Mishra, R. Geeta, Two unusual conjugated fatty acids,
532 parinaric acid and α-eleostearic acid, are present in several *Impatiens* species, but not in congener
533 *Hydrocera triflora*, Physiology and Molecular Biology of Plants 28(5) (2022) 1109-1118.
534 [13] M.A. Shabbir, M.R. Khan, M. Saeed, I. Pasha, A.A. Khalil, N. Siraj, Punicic acid: A striking
535 health substance to combat metabolic syndromes in humans, Lipids in Health and Disease 16(1) (2017)
536 99.
537 [14] B. Yang, H. Chen, C. Stanton, R.P. Ross, H. Zhang, Y.Q. Chen, W. Chen, Review of the roles of
538 conjugated linoleic acid in health and disease, Journal of Functional Foods 15 (2015) 314-325.
539 [15] H.J. Heipieper, R. Diefenbach, H. Keweloh, Conversion of *cis* unsaturated fatty acids to *trans*, a
540 possible mechanism for the protection of phenol-degrading *Pseudomonas putida* P8 from substrate
541 toxicity, Applied and Environmental Microbiology 58(6) (1992) 1847-1852.
542 [16] H. Keweloh, H.J. Heipieper, *Trans* unsaturated fatty acids in bacteria, Lipids 31(2) (1996) 129-
543 137.
544 [17] R. Holtwick, F. Meinhardt, H. Keweloh, *Cis-trans* isomerization of unsaturated fatty acids:
545 Cloning and sequencing of the *cti* gene from *Pseudomonas putida* P8, Applied and Environmental
546 Microbiology 63(11) (1997) 4292-4297.
547 [18] R. Holtwick, H. Keweloh, F. Meinhardt, *Cis*/*trans* isomerase of unsaturated fatty acids of
548 *Pseudomonas putida* P8: Evidence for a heme protein of the cytochrome *c* type, Applied and

549 Environmental Microbiology 65(6) (1999) 2644-2649.
550 [19] H.J. Heipieper, G. Meulenbeld, Q. van Oirschot, J. de Bont, Effect of environmental factors on
551 the *trans*/*cis* ratio of unsaturated fatty acids in *Pseudomonas putida* S12, Applied and Environmental
552 Microbiology 62(8) (1996) 2773-2777.
553 [20] F. Junker, L. Ramos Juan, Involvement of the *cis*/*trans* isomerase Cti in solvent resistance of
554 *Pseudomonas putida* DOT-T1E, Journal of Bacteriology 181(18) (1999) 5693-5700.
555 [21] H. Okuyama, A. Ueno, D. Enari, N. Morita, T. Kusano, Purification and characterization of 9-
556 hexadecenoic acid *cis-trans* isomerase from *Pseudomonas* sp. strain E-3, Archives of Microbiology
557 169(1) (1997) 29-35.
558 [22] V. Pedrotta, B. Witholt, Isolation and characterization of the *cis-trans*-unsaturated fatty acid
559 isomerase of *Pseudomonas oleovorans* GPo12, Journal of Bacteriology 181(10) (1999) 3256-3261.
560 [23] P.I. Nikel, V. de Lorenzo, *Pseudomonas putida* as a functional chassis for industrial biocatalysis:
561 From native biochemistry to *trans*-metabolism, Metabolic Engineering 50 (2018) 142-155.
562 [24] A. Weimer, M. Kohlstedt, D.C. Volke, P.I. Nikel, C. Wittmann, Industrial biotechnology of
563 *Pseudomonas putida*: Advances and prospects, Applied Microbiology and Biotechnology 104(18)
564 (2020) 7745-7766.
565 [25] Z. Tan, J.M. Yoon, D.R. Nielsen, J.V. Shanks, L.R. Jarboe, Membrane engineering via *trans*
566 unsaturated fatty acids production improves *Escherichia coli* robustness and production of
567 biorenewables, Metabolic Engineering 35 (2016) 105-113.
568 [26] K.E. Nelson, C. Weinel, I.T. Paulsen, R.J. Dodson, H. Hilbert, V.A.P. Martins dos Santos, D.E.
569 Fouts, S.R. Gill, M. Pop, M. Holmes, L. Brinkac, M. Beanan, R.T. DeBoy, S. Daugherty, J. Kolonay,
570 R. Madupu, W. Nelson, O. White, J. Peterson, H. Khouri, I. Hance, P.C. Lee, E. Holtzapple, D. Scanlan,
571 K. Tran, A. Moazzez, T. Utterback, M. Rizzo, K. Lee, D. Kosack, D. Moestl, H. Wedler, J. Lauber, D.
572 Stjepandic, J. Hoheisel, M. Straetz, S. Heim, C. Kiewitz, J. Eisen, K.N. Timmis, A. Düsterhöft, B.
573 Tümmler, C.M. Fraser, Complete genome sequence and comparative analysis of the metabolically

574 versatile *Pseudomonas putida* KT2440, Environmental Microbiology 4(12) (2002) 799-808.
575 [27] M. Fernández, S. Conde, J. de la Torre, C. Molina-Santiago, J.-L. Ramos, E. Duque, Mechanisms
576 of resistance to chloramphenicol in *Pseudomonas putida* KT2440, Antimicrobial Agents and
577 Chemotherapy 56(2) (2012) 1001-1009.
578 [28] J.-Y. Park, K.-M. Park, Y. Yoo, H. Yu, C.J. Lee, H.-S. Jung, K. Kim, P.-S. Chang, Catalytic
579 characteristics of a *sn*-1(3) regioselective lipase from *Cordyceps militaris*, Biotechnology Progress
580 35(e2744) (2019) 1-9.
581 [29] J.-Y. Park, C.H. Kim, Y. Choi, K.-M. Park, P.-S. Chang, Catalytic characterization of
582 heterodimeric linoleate 13*S*-lipoxygenase from black soybean (*Glycine max* (L.) Merr.), Enzyme and
583 Microbial Technology 139 (2020) 109595.
584 [30] J.J. Almagro Armenteros, K.D. Tsirigos, C.K. Sønderby, T.N. Petersen, O. Winther, S. Brunak, G.
585 von Heijne, H. Nielsen, SignalP 5.0 improves signal peptide predictions using deep neural networks,
586 Nature Biotechnology 37(4) (2019) 420-423.
587 [31] M. Baek, F. DiMaio, I. Anishchenko, J. Dauparas, S. Ovchinnikov, G.R. Lee, J. Wang, Q. Cong,
588 L.N. Kinch, R.D. Schaeffer, C. Millán, H. Park, C. Adams, C.R. Glassman, A. DeGiovanni, J.H.
589 Pereira, A.V. Rodrigues, A.A. van Dijk, A.C. Ebrecht, D.J. Opperman, T. Sagmeister, C. Buhlheller, T.
590 Pavkov-Keller, M.K. Rathinaswamy, U. Dalwadi, C.K. Yip, J.E. Burke, K.C. Garcia, N.V. Grishin,
591 P.D. Adams, R.J. Read, D. Baker, Accurate prediction of protein structures and interactions using a
592 three-track neural network, Science 373(6557) (2021) 871-876.
593 [32] E.F. Pettersen, T.D. Goddard, C.C. Huang, G.S. Couch, D.M. Greenblatt, E.C. Meng, T.E. Ferrin,
594 UCSF chimera—A visualization system for exploratory research and analysis, Journal of
595 Computational Chemistry 25(13) (2004) 1605-1612.
596 [33] M. Mauger, C. Ferreri, C. Chatgilialoglu, M. Seemann, The bacterial protective armor against
597 stress: The *cis-trans* isomerase of unsaturated fatty acids, a cytochrome-*c* type enzyme, Journal of
598 Inorganic Biochemistry 224 (2021) 111564.

[34] L. Thöny-Meyer, Biogenesis of respiratory cytochromes in bacteria, Microbiology and Molecular Biology Reviews 61(3) (1997) 337-376.

[35] S.H. Hristova, A.M. Zhivkov, Isoelectric point of free and adsorbed cytochrome *c* determined by various methods, Colloids and Surfaces B: Biointerfaces 174 (2019) 87-94.

[36] J. Muñoz-Rojas, P. Bernal, E. Duque, P. Godoy, A. Segura, J.-L. Ramos, Involvement of cyclopropane fatty acids in the response of *Pseudomonas putida* KT2440 to freeze-drying, Applied and Environmental Microbiology 72(1) (2006) 472-477.

[37] K. Kuhnt, M. Baehr, C. Rohrer, G. Jahreis, *Trans* fatty acid isomers and the *trans*-9/*trans*-11 index in fat containing foods, European Journal of Lipid Science and Technology 113(10) (2011) 1281-1292.

[38] E. Guillocheau, C. Penhoat, G. Drouin, A. Godet, D. Catheline, P. Legrand, V. Rioux, Current intakes of *trans*-palmitoleic (*trans*-C16:1 n-7) and *trans*-vaccenic (*trans*-C18:1 n-7) acids in France are exclusively ensured by ruminant milk and ruminant meat: A market basket investigation, Food Chemistry: X 5 (2020) 100081.

[39] C. Chatgilialoglu, C. Ferreri, M. Melchiorre, A. Sansone, A. Torreggiani, Lipid geometrical isomerism: From chemistry to biology and diagnostics, Chemical Reviews 114(1) (2014) 255-284.

[40] P. Delmonte, A.-R.F. Kia, Q. Hu, J.I. Rader, Review of methods for preparation and gas chromatographic separation of *trans* and *cis* reference fatty acids, Journal of AOAC INTERNATIONAL 92(5) (2009) 1310-1326.

[41] J.-Y. Park, Y.-S. Jung, D. Charalampopoulos, K.-M. Park, P.-S. Chang, Controlling *cis*/*trans* isomerism of monounsaturated fatty acids via a recombinant cytochrome *c*-type *cis*/*trans* fatty acid isomerase, Food Control 160 (2024) 110319.

[42] M. Santiago, C.A. Ramírez-Sarmiento, R.A. Zamora, L.P. Parra, Discovery, molecular mechanisms, and industrial applications of cold-active enzymes, Frontiers in Microbiology 7(1408) (2016) 1-32.

[43] A. von Wallbrunn, H. Richnow Hans, G. Neumann, F. Meinhardt, J. Heipieper Hermann,

624 Mechanism of *cis-trans* isomerization of unsaturated fatty acids in *Pseudomonas putida*, Journal of
625 Bacteriology 185(5) (2003) 1730-1733.
626 [44] A. Bonamore, A. Farina, M. Gattoni, M.E. Schininà, A. Bellelli, A. Boffi, Interaction with
627 membrane lipids and heme ligand binding properties of *Escherichia coli* flavohemoglobin,
628 Biochemistry 42(19) (2003) 5792-5801.
629 [45] P. D'Angelo, D. Lucarelli, S. della Longa, M. Benfatto, J.L. Hazemann, A. Feis, G. Smulevich,
630 A. Ilari, A. Bonamore, A. Boffi, Unusual heme iron-lipid acyl chain coordination in *Escherichia coli*
631 flavohemoglobin, Biophysical Journal 86(6) (2004) 3882-3892.
632 [46] C. Eberlein, T. Baumgarten, S. Starke, H.J. Heipieper, Immediate response mechanisms of Gram-
633 negative solvent-tolerant bacteria to cope with environmental stress: *Cis-trans* isomerization of
634 unsaturated fatty acids and outer membrane vesicle secretion, Applied Microbiology and
635 Biotechnology 102(6) (2018) 2583-2593.
636

Table 1. Purification chart of *cis*/*trans* fatty acid isomerase (CTI) from the periplasmic fraction of *Pseudomonas putida* KT2440

Step	Total volume[1] (mL)	Total protein (mg)	Total activity[2] (units, U)	Specific activity (mU/mg)
Periplasmic extraction	2000.00	960.00	2.03	3.19
60% $(NH_4)_2SO_4$ precipitation	35.00	831.04	1.79	3.39
HiTrap® Q Fast Flow anion exchange chromatography	11.00	173.01	0.38	7.01
HiTrap® DEAE Fast Flow anion exchange chromatography	7.00	24.09	0.14	19.55
HiPrep™ 16/60 Sephacryl® S-100 HR size exclusion chromatography	3.00	0.18	0.04	351.94

[1]The periplasmic fraction was extracted from a total of 80 g of *P. putida* KT2440 cells (dry weight, 4 batches), as described in M
[2]The CTI activity was evaluated with palmitoleic acid ($C_{16:1}$, *cis*-Δ^9), as described in Materials & Methods.

Figure captions

Fig. 1. Serial chromatographic purification of wild-type *cis*/*trans* fatty acid isomerase (CTI) from the periplasmic fraction of *Pseudomonas putida* KT2440. (a) HiTrap® Q Fast Flow (FF) anion exchange chromatography. (b) HiTrap® DEAE FF anion exchange chromatography. (c) HiPrep™ 16/60 Sephacryl® S-100 HR size exclusion chromatography. Proteins in each eluted fraction were detected by measuring the absorbance at 280 nm wavelength. The eluted fractions were dialyzed into 50 mM potassium phosphate buffer (pH 7.5), and the CTI activity was evaluated against palmitoleic acid as a substrate.

Fig. 2. Structural identification of wild-type *cis*/*trans* fatty acid isomerase (CTI) from *Pseudomonas putida* KT2440. (a) Analytical size exclusion chromatography of the purified CTI. A calibration curve for estimating the molecular weight was derived using five standard proteins: thyroglobulin from bovine thyroid gland (670 kDa), γ-globulin from bovine blood (150 kDa), ovalbumin (44.3 kDa), ribonuclease A type I-A (13.7 kDa), and *p*-aminobenzoic acid (0.137 kDa). V_e, the peak elution volume of protein; V_o, the void volume of column. (b) SDS-PAGE analysis of eluted proteins in each purification step. A single thick protein band containing putative CTIs was detected in a highly purified sample. M, protein molecular marker; Lane 1, crude periplasmic extracts; Lane 2, unbound fractions (integrated 2–3 fractions, 1.0 mL/fraction) from HiTrap® Q Fast Flow (FF) anion exchange chromatography; Lane 3, unbound fractions (integrated 2–3 fractions, 1.0 mL/fraction) from HiTrap® DEAE FF anion exchange chromatography; Lane 4, eluted fractions (integrated 44–51 fractions, 0.5 mL/fraction) from HiPrep™ 16/60 Sephacryl® S-100 HR size exclusion chromatography.

Fig. 3. Isomerization of monounsaturated fatty acids by wild-type *cis*/*trans* fatty acid isomerase (CTI) from *Pseudomonas putida* KT2440. (a) The GC-FID chromatograms of the reactants before (dash line)

and after (straight line) the 30 min CTI reaction against 1 mM palmitoleic acid ($C_{16:1}$, *cis*-Δ^9). Both the substrates and the products in the reactants were fully methylated before GC-FID analysis. (b) Time-course of the production of *trans*-fatty acids from each *cis*-fatty acid (substrate) until reaction equilibration (120 min). PEA, palmitelaidic acid ($C_{16:1}$, *trans*-Δ^9); VA, vaccenic acid ($C_{18:1}$, *trans*-Δ^{11}); EA, elaidic acid ($C_{18:1}$, *trans*-Δ^9). (c) Final conversion rates (%) of *cis* configuration to *trans* configuration from the CTI reactions. POA, palmitoleic acid; cVA, *cis*-vaccenic acid ($C_{18:1}$, *cis*-Δ^{11}); OA, oleic acid ($C_{18:1}$, *cis*-Δ^9). Asterisk denotes significant differences between the data ($p<0.05$).

Fig. 4. Enzyme kinetic analysis of wild-type *cis*/*trans* fatty acid isomerase (CTI) from *Pseudomonas putida* KT2440 against palmitoleic acid ($C_{16:1}$, *cis*-Δ^9). (a) Michaelis-Menten plot of the CTI reaction. The initial velocity (v) at each substrate concentration (0.10–1.20 mM) was derived from a linear regression of the time-course CTI reaction (0–30 min). (b) Hanes-Woolf double-reciprocal plot of the reaction. All the CTI reactions (triplicate) were conducted at the optimal reaction pH and temperature.

Fig. 5. Computational prediction of the structure of wild-type *cis*/*trans* fatty acid isomerase (CTI) from *Pseudomonas putida* KT2440. (a) Structural features of CTI. The CTI has a conserved cytochrome *c*-type domain with an iron-containing heme binding motif (CVACH), as well as a Sec/SP1 signal peptide (1−20 residues) at the N-terminus. (b) Prediction of signal peptide (SP) and cleavage site (CS) of CTI. The likelihoods of signal peptide were expressed as region probabilities (P). (c) Predicted three-dimensional protein structure model of CTI. Two cysteine residues (C_{43} and C_{46}) of the heme-binding motif can be covalently linked to a heme C molecule by two thioether bonds after cytochrome *c* maturation. (For interpretation of the color, the reader should be referred to the web version of this paper.)

Fig. 6. Proposed molecular mechanism of substrate specificity of wild-type *cis*/*trans* fatty isomerase (CTI) from *P*. *putida* KT2440. The predicted structure of the cytochrome *c*-type catalytic domain of CTI was represented by its molecular surface and colored according to the degree of hydrophobicity. (For interpretation of the color, the reader should be referred to the web version of this paper.)

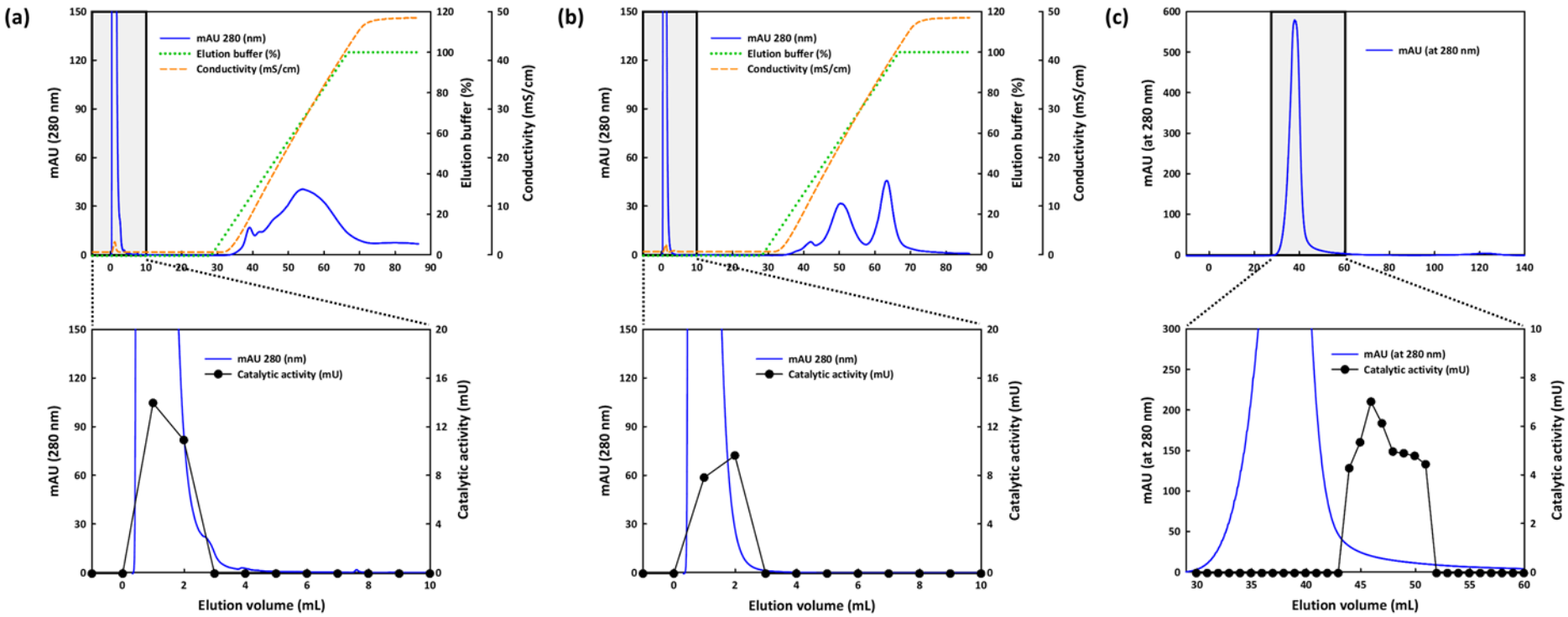
(a)
(b)
(c)
mAU 280 (nm)
Elution buffer (%)
Conductivity (mS/cm)
mAU (280 nm)
Elution buffer (%)
Conductivity (mS/cm)
mAU 280 (nm)
Catalytic activity (mU)
mAU (280 nm)
Catalytic activity (mU)
Elution volume (mL)
mAU (at 280 nm)
mAU (at 280 nm)
Catalytic activity (mU)
mAU (at 280 nm)
Catalytic activity (mU)
Elution volume (mL)

Fig. 1.

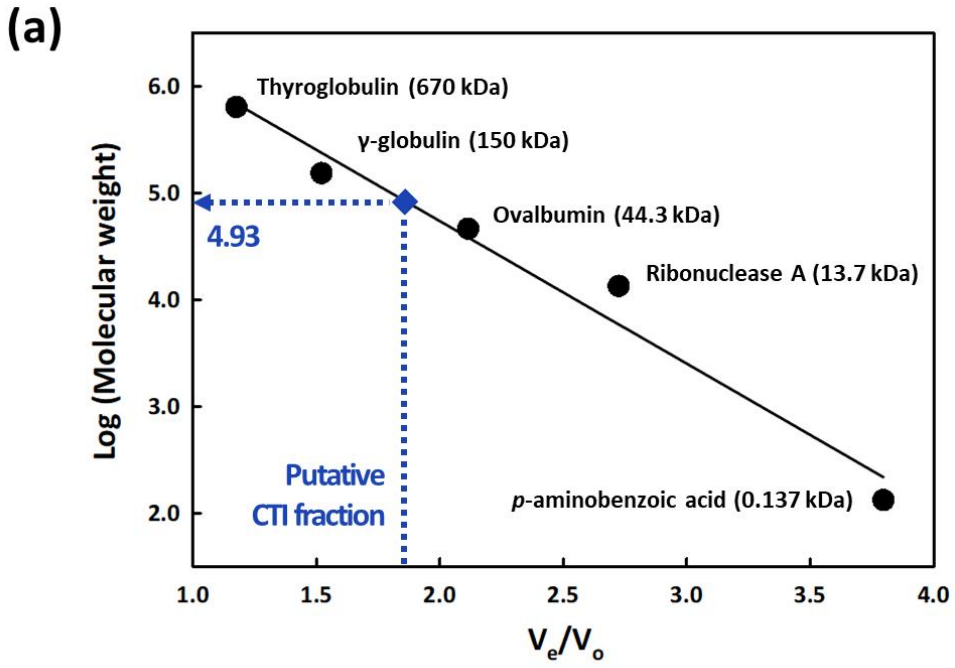
(a)
Thyroglobulin (670 kDa)
γ-globulin (150 kDa)
Ovalbumin (44.3 kDa)
Ribonuclease A (13.7 kDa)
p-aminobenzoic acid (0.137 kDa)
4.93
Putative
CTI fraction
Log (Molecular weight)
6.0
5.0
4.0
3.0
2.0
1.0
1.5
2.0
2.5
3.0
3.5
4.0
Ve/Vo

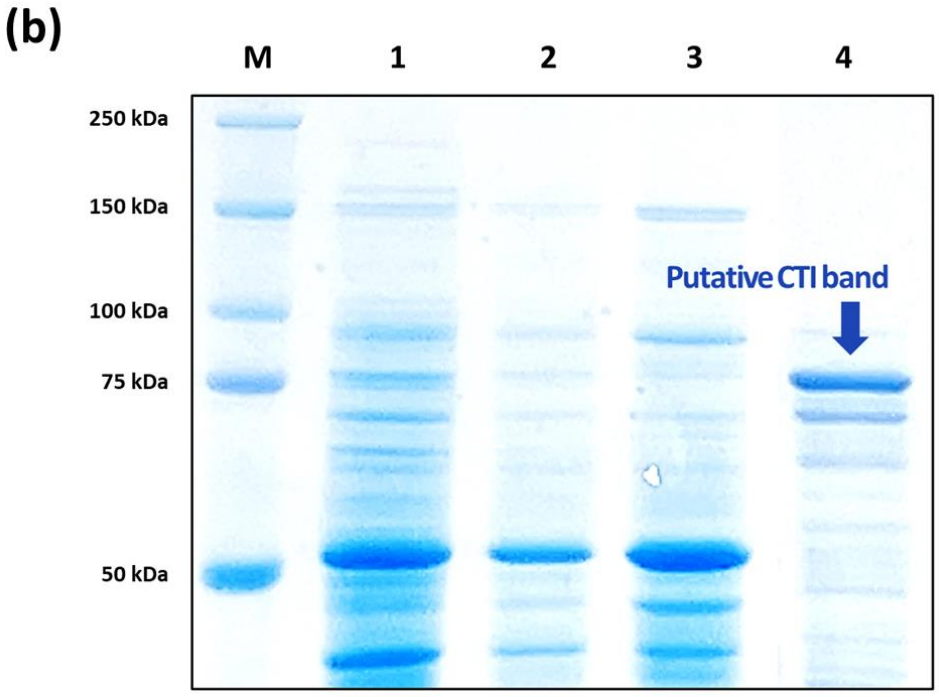
(b)
M
1
2
3
4
250 kDa
150 kDa
100 kDa
75 kDa
50 kDa
Putative CTI band

Fig. 2.

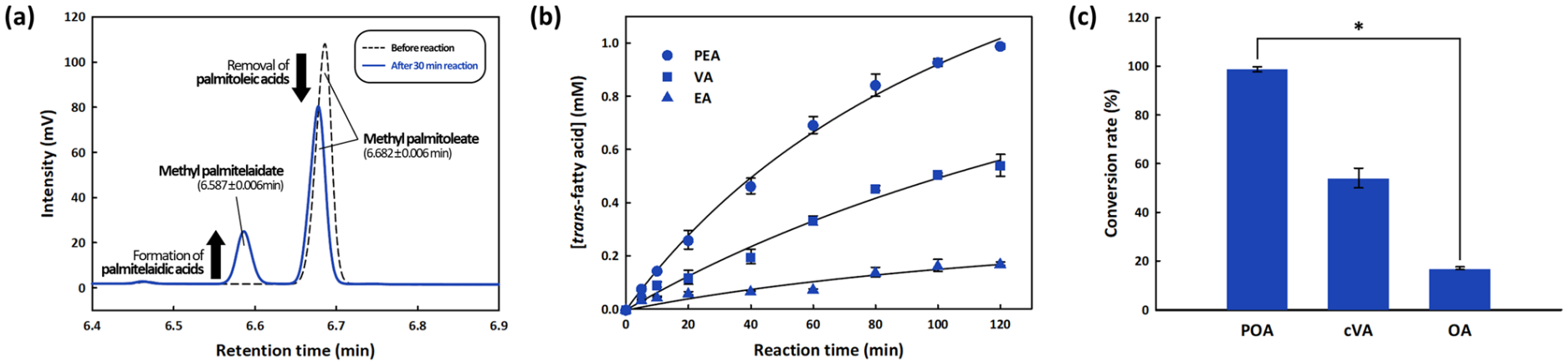
(a)
Intensity (mV)
Retention time (min)
Before reaction
After 30 min reaction
Removal of palmitoleic acids
Methyl palmitoleate (6.682±0.006 min)
Methyl palmitelaidate (6.587±0.006min)
Formation of palmitelaidic acids
(b)
[trans-fatty acid] (mM)
Reaction time (min)
PEA
VA
EA
(c)
Conversion rate (%)
*
POA
cVA
OA

Fig. 3.

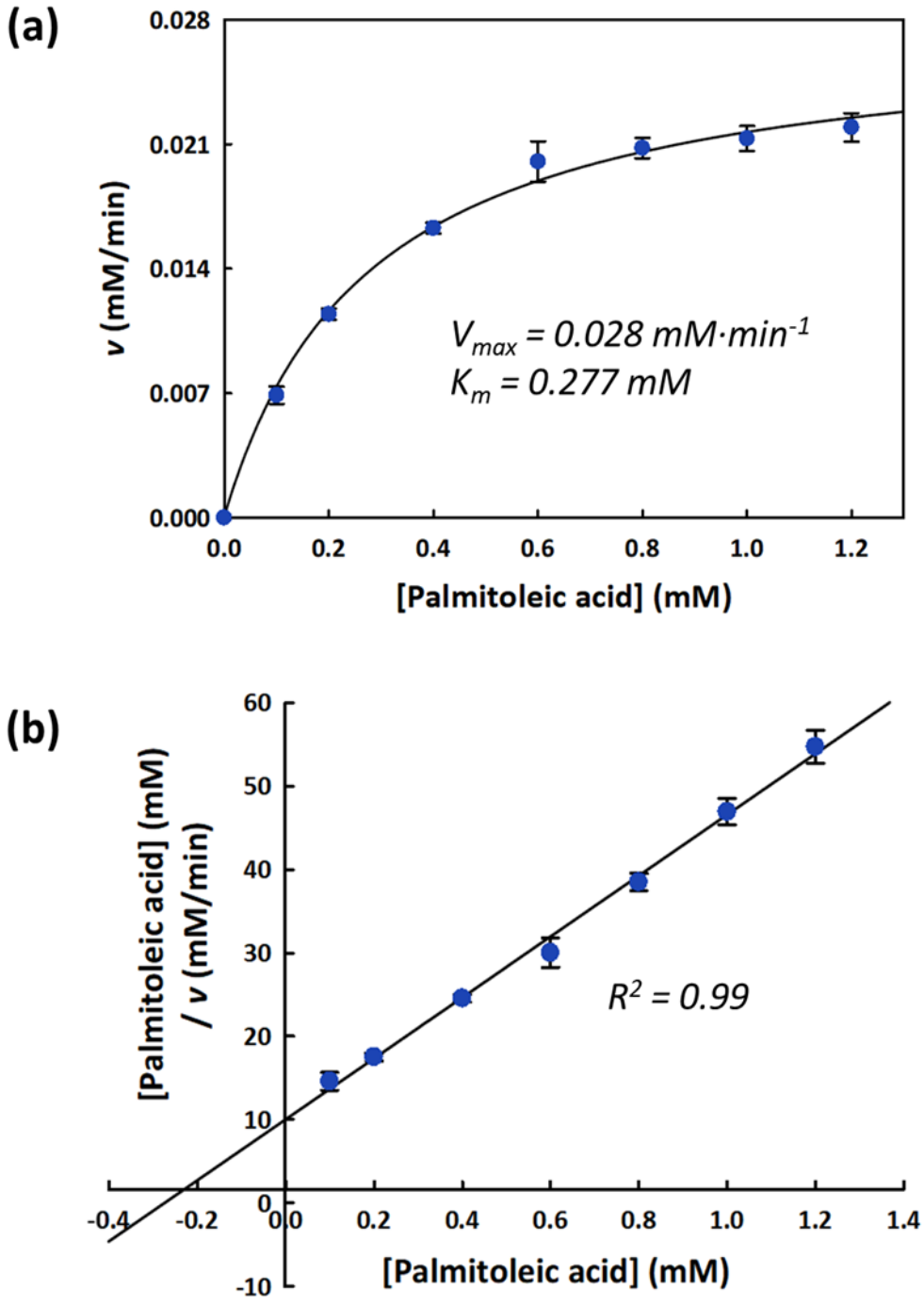
(a)
0.028
0.021
0.014
0.007
0.000
v (mM/min)
V_{max} = 0.028 mM·min^{-1}
K_m = 0.277 mM
0.0
0.2
0.4
0.6
0.8
1.0
1.2
[Palmitoleic acid] (mM)
(b)
60
50
40
30
20
10
0
-10
[Palmitoleic acid] (mM) / v (mM/min)
R^2 = 0.99
-0.4
-0.2
0.0
0.2
0.4
0.6
0.8
1.0
1.2
1.4
[Palmitoleic acid] (mM)

Fig. 4.

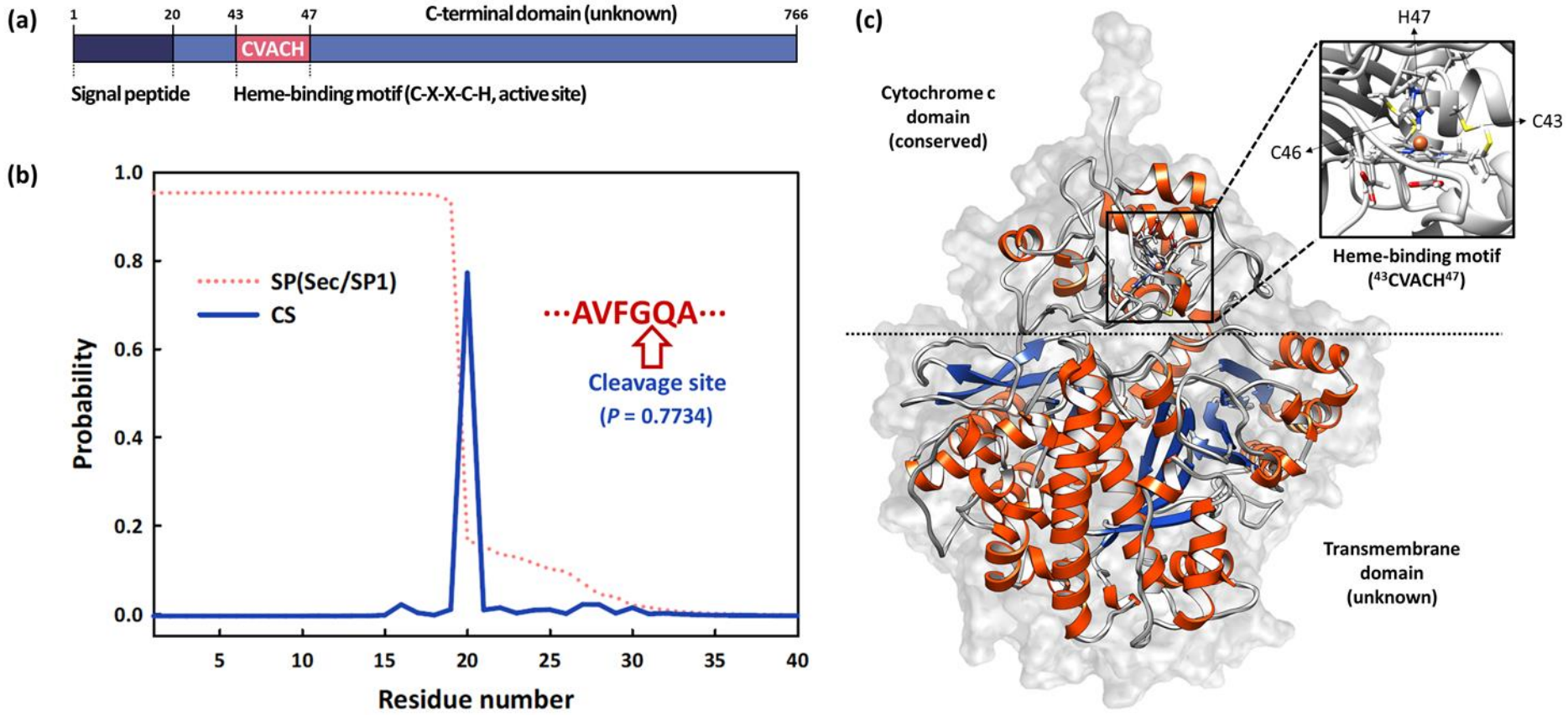
(a)
1
20
43
47
C-terminal domain (unknown)
766
CVACH
Signal peptide
Heme-binding motif (C-X-X-C-H, active site)
(b)
1.0
0.8
0.6
0.4
0.2
0.0
Probability
SP(Sec/SP1)
CS
···AVFGQA···
Cleavage site
(P = 0.7734)
5
10
15
20
25
30
35
40
Residue number
(c)
Cytochrome c
domain
(conserved)
H47
C43
C46
Heme-binding motif
(43CVACH47)
Transmembrane
domain
(unknown)

Fig. 5.

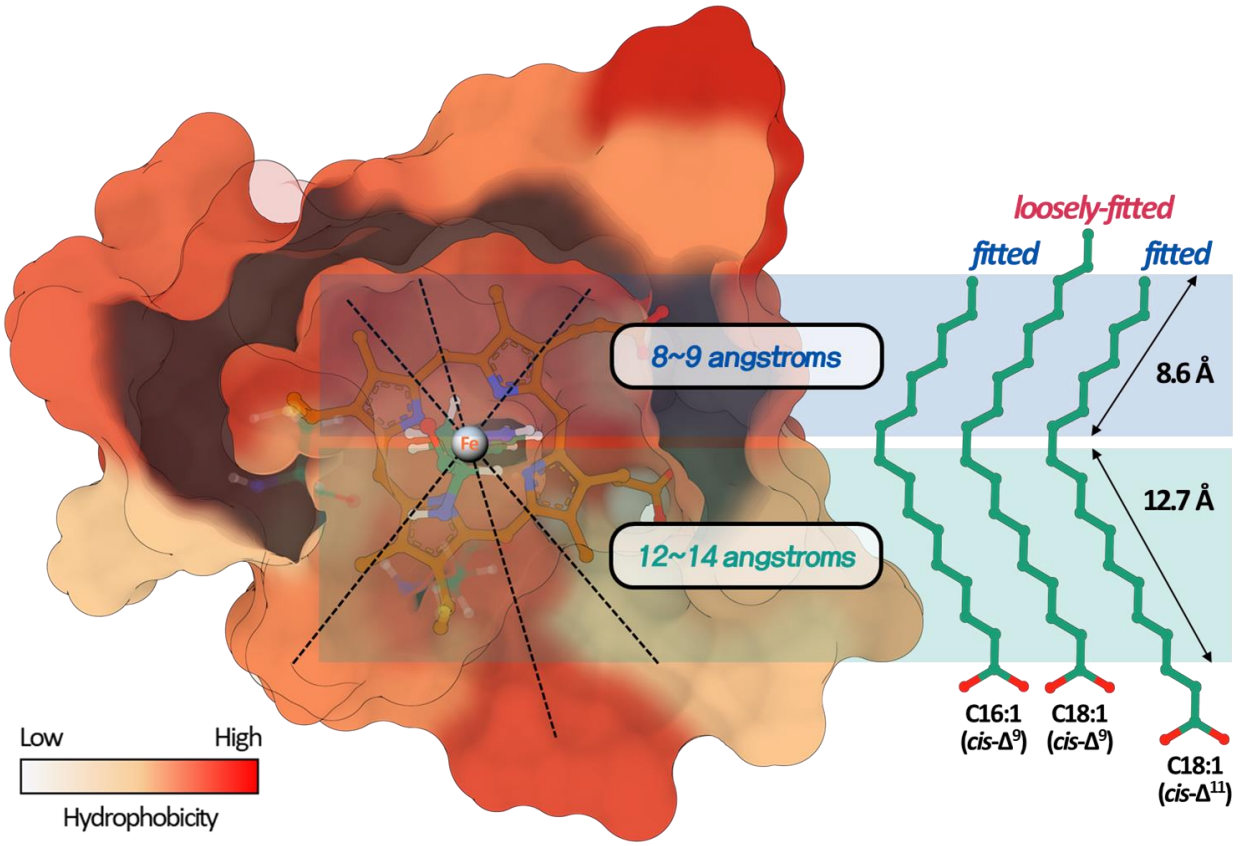
loosely-fitted
fitted
fitted
8~9 angstroms
12~14 angstroms
8.6 Å
12.7 Å
Fe
Low
High
Hydrophobicity
C16:1
(cis-Δ9)
C18:1
(cis-Δ9)
C18:1
(cis-Δ11)

Fig. 6.